ACS Sustainable Chemistry & Engineering

Research Article

pubs.acs.org/journal/ascecg

$NbSe_2$ Nanosheet Supported $PbBiO_2Br$ as a High Performance Photocatalyst for the Visible Light-driven Asymmetric Alkylation of Aldehyde

Xiaojie Li, Jun Wang, Danyun Xu, Zhen Sun, Qingshan Zhao, Wenchao Peng, Yang Li, Guoliang Zhang, Fengbao Zhang, and Xiaobin Fan*

State Key Laboratory of Chemical Engineering, Key Laboratory for Green Chemical Technology, School of Chemical Engineering & Technology, Collaborative Innovation Center of Chemical Science and Engineering, Tianjin University, Tianjin 300072, China

Supporting Information

ABSTRACT: Visible light photoredox catalysis has been demonstrated to be a promising and green strategy for organic synthesis. In this study, a nanocomposite of $PbBiO_2Br$ nanoparticles and $NbSe_2$ nanosheet was prepared as a high performance photocatalyst for the visible light-driven asymmetric alkylation of aldehyde. It was found that the introduction of a small amount of $NbSe_2$ (0.5 wt %) to the $PbBiO_2Br$ semiconductor could result in ~50% increase in the yield of the final product. This study shows that $NbSe_2$ nanosheets can be used as an efficient support to suppress the recombination of photoinduced electron−hole pairs and contribute to the enhanced photocatalytic performances of semiconductors in the visible light-driven catalysis.

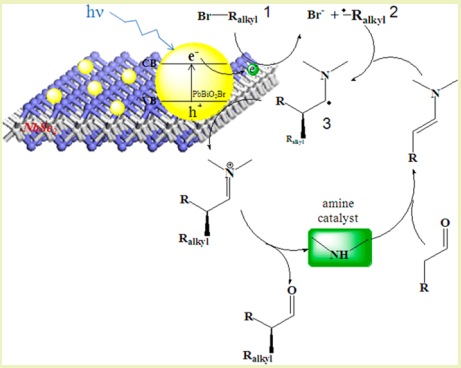

KEYWORDS: *Photocatalysis, Two-dimensional nanosheet, $NbSe_2$, Organic synthesis, Asymmetric alkylation*

INTRODUCTION

Visible light photoredox catalysis is currently the subject of intense research in organic synthesis.[1−10] Combining the photoinduced organic synthesis with organocatalysis has been demonstrated to be an efficient and green strategy for the asymmetric synthesis.[11−14] For example, a series of asymmetric catalytic reactions,[11,15,16] such as the direct α-alkylation of aldehydes[11] have been successfully employed to prepare a variety of important organic compounds. In most of these studies, homogeneous transition-metal complexes, especially the Ir(III) and Ru(II) complexes, are employed as photocatalysts.[11,15−22] Despite their high efficiency, the practical applications of these photocatalysts are hampered by their high costs and the difficulty in separation from the reaction mixtures.[23] The ability to recover and reuse the photocatalysts involved can not only eliminate the contamination of the organic products but also reduce the waste disposal cost in large-scale reactions. Therefore, some inorganic semiconductors with photooxidation properties under visible-light irradiation have been explored as cheap and recyclable photocatalysts in asymmetric synthesis.[24,25] For example, $PbBiO_2Br$, with an optical band gap of 2.56 eV, is one of the most promising photocatalysts for the alkylation of aldehydes.[24] However, these heterogeneous semiconductors often suffer from lower efficiency when compared with the homogeneous metal complexes, due to the recombination of photogenerated electron−hole pairs,[26−32] their agglomeration,[33,34] as well as the mass transfer limitation[23,35−38] we have demonstrated before.

In this study, we propose a novel $PbBiO_2Br$−SOF-$NbSe_2$ nanocomposite that shows much better catalytic performance than $PbBiO_2Br$ in the visible light-driven asymmetric α-alkylation of aldehydes reaction. It was found that the two-dimensional (2D) single-layer or few-layer $NbSe_2$ (SOF-$NbSe_2$) nanosheet with high specific surface area and metallic properties[39−42] could be used as a promising support and electron transfer station to enhance the separation of photogenerated electron−hole pairs (see Scheme 1 for an image of the proposed mechanism).

EXPERIMENTAL SECTION

Materials. The $NbSe_2$ powder was purchased from InnoChem Science & Technology Co., Ltd. (Beijing, China). Bromodiethymalonate (90%), octanal (98%) and 2,6-lutidine (98%) were purchased from Heowns biochemical Technology Co., Ltd. (Tianjin, China). All other materials were commercially available and used without further purification.

Synthesis of $PbBiO_2Br$−SOF-$NbSe_2$ Nanocomposite and Amine Catalyst. SOF-$NbSe_2$ was prepared by Zhang's method: electrochemical lithium intercalation.[40,43] $PbBiO_2Br$ was obtained by Cherevatskaya's process.[24] Both SOF-$NbSe_2$ and $PbBiO_2Br$ (100 mg) with different mass ratios (SOF-$NbSe_2$/$PbBiO_2Br$ = 0.2%, 0.5%, 1%,

Received: March 6, 2015
Revised: April 7, 2015
Published: April 15, 2015

DOI: 10.1021/acssuschemeng.5b00182
ACS Sustainable Chem. Eng. 2015, 3, 1017−1022

Scheme 1. Illustration for the Process and Proposed Mechanism of the Enantioselective α-Alkylation of Aldehydes Catalyzed by $PbBiO_2Br$–SOF-$NbSe_2$ Nanocomposites under Blue LED Illumination[a]

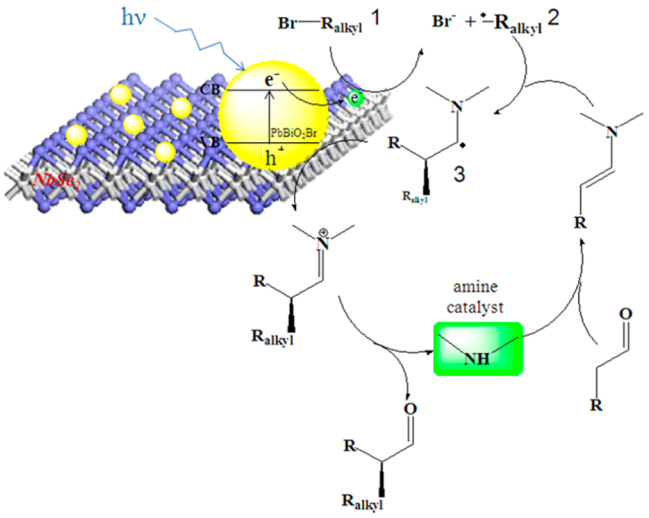

[a](R_{alkyl} = $C(COOCH_2)_2$, R = $(CH_2)_5CH_3$).

2%) were added into CH_3CN (4 mL), followed by ultrasonic treatment for 5 min. Then the suspension was stirred with a magnetic stirrer in a test tube (10 mL) for 12 h. The resultant composite was collected by centrifugation (12000*g*, 10 min), washed repeatedly with ethanol and deionized water, and freeze-dried in a vacuum. (2*R*,5*S*)-2-*tert*-butyl-3,5-dimethylimidazolidin-4-one was synthesized according to MacMillan's method[44] and used as the auxiliary catalyst.

Photocatalytic Experiments. The reactions were carried out in a 10 mL Schlenk tube equipped with a magnetic stirrer at 20 °C. The nanocomposite (50 mg) or $PbBiO_2Br$ (50 mg) and auxiliary catalyst (33 mg, 156 μmol) were added into the tube. Into the glovebox was placed the tube. Then bromodiethymalonate (133 μL, 0.78 mmol), octanal (305 μL, 1.95 mmol), 2,6-lutidine (182 μL, 1.56 mmol) and acetonitrile (2.5 mL) were added into the tube. The tube was taken out and sonicated for 2 min. The resulting mixture was vigorously stirred under blue LED light (4 W). After 20 h, the catalyst was separated by sedimentation, and the supernatant was filtrated and analyzed by gas chromatography (GC). The recovered catalyst was washed with ethanol and deionized water, freeze-dried under vacuum and then reused for the above reaction.

Fabrication of Film Electrodes and Electrochemical Impedance Spectra (EIS) Measurements. For the EIS measurement, $PbBiO_2Br$ and $PbBiO_2Br$–SOF-$NbSe_2$ powders were fabricated as film electrodes by a method reported in previous work.[26,45] First, the powders and ethanol were mixed homogeneously (150 mg/mL), and the obtained paste was then spread on the conducting fluorine-doped SnO_2 glass substrate (FTO 15 Ω/square) with a glass rod, using adhesive tapes as spacers. Finally, the resultant films with a ca. 4 μm thickness and 1 cm^2 active area were calcinated at 450 °C for 2 h in N_2 atmosphere to achieve good electronic contact between the particles.

The EIS measurements were carried out on an electrochemical workstation (Chenhua Chi660E) by using three-electrode cells. The resultant electrode served as the working electrode, with a platinum wire as the counter electrode and an Ag/AgCl (saturated KCl) electrode as the reference electrodes. The measurement was performed in the presence of a 2.5 mM $K_3[Fe(CN)_6]/K_4[Fe(CN)_6]$ (1:1) mixture as a redox probe in 0.1 M KCl solution. The impedance spectra were recorded in the mode of AC impedance under an AC perturbation signal of 5 mV over the frequency range of 1 MHz to 100 mHz.

Materials Characterizations. The samples were characterized by scanning electron microscopy (SEM) (Hitachi S4800), transmission electron microscopy (TEM) (Philips Tecnai G2 F20), energy-dispersive X-ray spectroscopy (EDX) (Philips Tecnai G2 F20), X-ray diffraction (XRD) (AXS D8-Focus), diffusion reflectance UV–visible (UV–vis) spectra (Unico UV-2800) and electrochemical impedance spectroscopy (EIS) (Chenhua Chi660E). The reaction results were measured by GC (Agilent 6890N GC-FID system). The purified products were characterized by nuclear magnetic resonance (NMR) (Varian Inova 400 MHz).

RESULTS AND DISCUSSION

Characterizations of $PbBiO_2Br$–SOF-$NbSe_2$ Nanocomposite. A SOF-$NbSe_2$ sheet was obtained by Zhang's electrochemical lithium intercalation method.[40,43] From Figure 1a, combined with Figure S1a of the Supporting Information, it

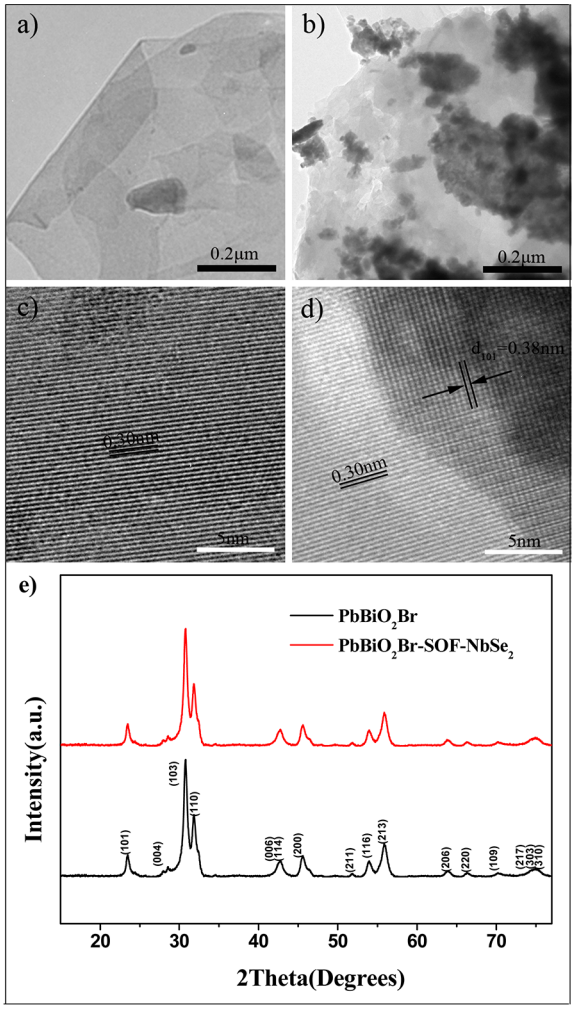

Figure 1. TEM images of (a) SOF-$NbSe_2$, (b) $PbBiO_2Br$–SOF-$NbSe_2$ nanocomposite. HRTEM images of (c) SOF-$NbSe_2$ and (d) $PbBiO_2Br$–SOF-$NbSe_2$ nanocomposite. (e) XRD patterns of $PbBiO_2Br$–SOF-$NbSe_2$ and $PbBiO_2Br$ alone.

can be seen that the SOF-$NbSe_2$ shows a sheet-like structure with micrometer-long wrinkles, which may be beneficial for the absorption of reactants.[26] The $PbBiO_2Br$–SOF-$NbSe_2$ nanocomposite was prepared by a simple blending strategy. In brief, $PbBiO_2Br$ nanoparticles and a small amount of SOF-$NbSe_2$ sheets were mixed and ultrasonicated in CH_3CN for 5 min, and the mixture was further stirred for 12 h. After centrifugation, washing and freeze-drying, the nanocomposite was obtained. Figure 1b, combined with Figure S1b of the Supporting Information, shows the typical TEM and SEM images of the

DOI: 10.1021/acssuschemeng.5b00182
ACS Sustainable Chem. Eng. 2015, 3, 1017–1022

$PbBiO_2Br$–SOF-$NbSe_2$ nanocomposite with a SOF-$NbSe_2$ loading of 0.5 wt %. It can be seen that the $PbBiO_2Br$ nanoparticles were dispersed on the SOF-$NbSe_2$ sheet, with many agglomerates on the 2D nanosheets. High-resolution transmission electron microscopy (HRTEM) reveals the lattice spacing of SOF-$NbSe_2$ is about 0.30 nm (Figure 1c,d), in line with a previous report,[40] whereas that of $PbBiO_2Br$ (Figure 1d) is about 0.38 nm, corresponding to the (101) atomic planes of the tetragonal structure of $PbBiO_2Br$. Interestingly, the $PbBiO_2Br$–SOF-$NbSe_2$ nanocomposite shows an identical X-ray diffraction (XRD) pattern of pure tetragonal structure $PbBiO_2Br$ (JCPDS Card No. 38-1008) (Figure 1e). The absence of peaks for $NbSe_2$ should be attributed to its low loading amount, as well as its exfoliated 2D structure. All of the results, combined with energy-dispersive X-ray spectroscopy (EDX) mapping (Figure S2 of the Supporting Information), demonstrate the successful preparation of $PbBiO_2Br$–SOF-$NbSe_2$ nanocomposite.

Diffuse reflectance UV–vis spectroscopy (Figure 2a) was applied to study the interaction between $PbBiO_2Br$ and SOF-

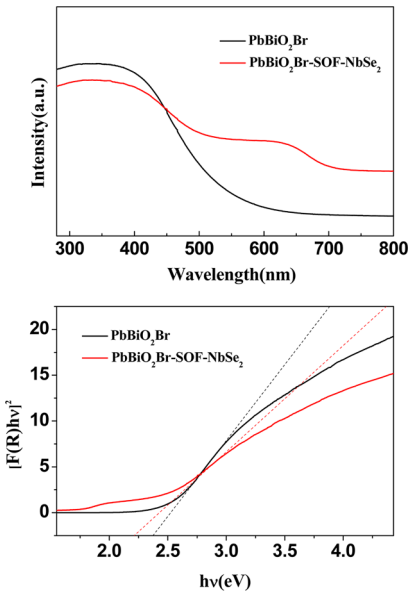

Figure 2. (a) Diffuse reflectance UV–vis spectra of $PbBiO_2Br$ and $PbBiO_2Br$–SOF-$NbSe_2$. (b) Corresponding plot of transformed Kubelka–Munk function versus the energy of light.

$NbSe_2$ in the $PbBiO_2Br$–SOF-$NbSe_2$ nanocomposite. The main absorption band of $PbBiO_2Br$ is in the range of 300–500 nm, whereas the presence of SOF-$NbSe_2$ leads to a continuous absorption in 500–700 nm, which is in agreement with the gray color of SOF-$NbSe_2$. Figure 2b shows the results of plot of transformed Kubelka–Munk function versus the energy of light, by which the roughly estimated band gaps are 2.45 and 2.54 eV, corresponding to $PbBiO_2Br$–0.5%SOF-$NbSe_2$ and bare $PbBiO_2Br$, respectively. The slight narrowing of the band gap (0.09 eV) is proposed to the formation of Se–Pb and Se–Bi bonds between $PbBiO_2Br$ and SOF-$NbSe_2$ (Scheme S1 of the Supporting Information), similar to that observed for the carbon-doped TiO_2 nanocomposites.[26,46]

Electrochemical impedance spectroscopy (EIS) was also carried out to further characterize the interactions between the $PbBiO_2Br$ and SOF-$NbSe_2$. As shown in Figure 3, the typical EIS of $PbBiO_2Br$ is presented as Nyquist plots, and the

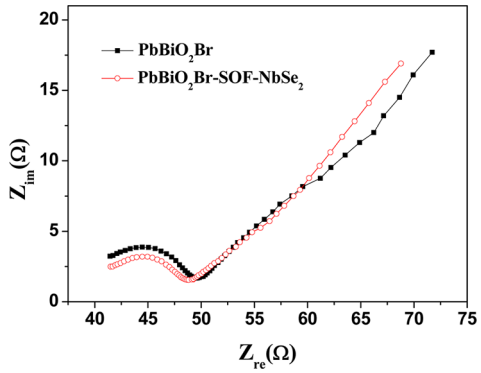

Figure 3. EIS changes of $PbBiO_2Br$ and $PbBiO_2Br$–SOF-$NbSe_2$ electrodes. EIS was performed in the presence of a 2.5 mM $K_3[Fe(CN)_6]/K_4[Fe(CN)_6]$(1:1) mixture as a redox probe in 0.1 M KCl aqueous solution.

introduction of SOF-$NbSe_2$ (despite its low loading) results in a shorter diameter of the semicircle, indicating a decrease in the solid state interface layer resistance[26,47] and a faster charge transfer in the $PbBiO_2Br$–SOF-$NbSe_2$ nanocomposite. This result is attributed to the metallic property of SOF-$NbSe_2$, which contributes to the suppression of charge recombination and a potential higher photocatalytical activity.

Photocatalytic Activity and Mechanism. To probe its potential applications in visible light photoredox catalysis, the enantioselective α-alkylation of aldehyde to synthesize (*R*)-diethyl 2-(1-oxohexan-2-yl)propanedioate was used as a model reaction. From Table 1, it can be seen that with the increase of

Table 1. Enantioselective Alkylations Using Different Mass Ratios of SOF-$NbSe_2$/$PbBiO_2Br$ as Photocatalyst

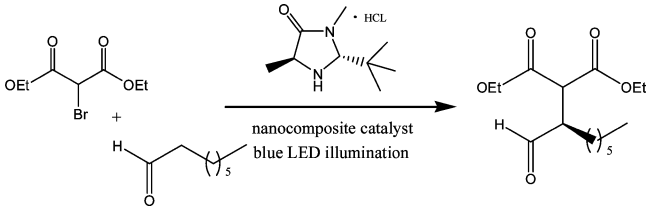

entry	(wt %)[a]	yield [%][b]	ee [%][c]
1	0	62.9	73
2	0. 2	67.8	76
3	0. 5	90.8	74
4	1	75.8	74
5	2	52.8	71

[a]Mass ratio of SOF-$NbSe_2$/$PbBiO_2Br$. [b]Yield of product. [c]Value of the enantiomeric excess determined by gas chromatography (GC) with chiral column.

the mass ratio of SOF-$NbSe_2$ to $PbBiO_2Br$, the yield of the product will have a decline trend after the initial ascent. The maximum yield of 90.8% could be achieved in the $PbBiO_2Br$–SOF-$NbSe_2$ composites with a SOF-$NbSe_2$-to-$PbBiO_2Br$ mass ratio of 0.005:1, whereas the yield of the product is only 62.9% with $PbBiO_2Br$ alone. It should be noted that the surface coverage of SOF-$NbSe_2$ by $PbBiO_2Br$ is estimated to be ~50% when the mass ratio of 0.005:1 was employed (Figure S3 of the Supporting Information). Combining these results and the UV–vis and EIS data above, it is proposed that the photoexcited electrons on the conduction band of $PbBiO_2Br$ (Figure S4 of the Supporting Information) could be transferred

DOI: 10.1021/acssuschemeng.5b00182
ACS Sustainable Chem. Eng. 2015, 3, 1017–1022

onto the metallic SOF-$NbSe_2$ sheet, leaving the holes on $PbBiO_2Br$ nanoparticles. Then, the electrons are cached by the bromodiethylmalonate to produce the alkyl radical, whereas SOF-$NbSe_2$ is oxidized by the holes of $PbBiO_2Br$. In this system, photoinduced electrons and holes can be effectively separated, and the photocatalytic efficiency is significantly increased. Besides that, the existence of SOF-$NbSe_2$ and the subsequent formation of interfaces between $PbBiO_2Br$ and SOF-$NbSe_2$ could provide more active sites for the former reaction, which may also be beneficial to the photoredox catalysis process.[48,49] However, it should be noted that only the modest loading of SOF-$NbSe_2$ could enhance the photocatalytical activity of the nanocomposite toward the reaction. Overloading of the SOF-$NbSe_2$ (the SOF-$NbSe_2$ to $PbBiO_2Br$ mass ratio above 0.005:1) could result in significant decrease in the catalytic performance, because excess SOF-$NbSe_2$ would block the transmission of visible light and reduce the light absorbance of $PbBiO_2Br$. (Figure S5 of the Supporting Information)

The stability and reusability of the $PbBiO_2Br$–SOF-$NbSe_2$ catalyst were tested by repeated experiments (Figure 4). It was

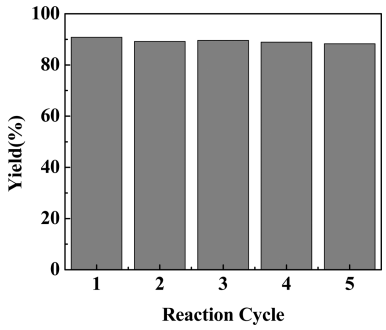

Figure 4. Recycling experiments for $PbBiO_2Br$–SOF-$NbSe_2$ composite catalyzed reaction.

demonstrated that the $PbBiO_2Br$–SOF-$NbSe_2$ nanocomposite could be reused for at least five cycles without distinct loss of its catalytic activity. In addition, the reused nanocomposite catalyst showed no obvious difference in morphology under TEM observations (Figure S6 of the Supporting Information). All these results show the good stability of the nanocomposite catalyst.

The performances of $PbBiO_2Br$–SOF-$NbSe_2$ nanocomposite in the alkylation of aldehyde of other substrates were also investigated, and the results are summarized in Table 2, which further demonstrated the efficiency of the nanocomposite.

CONCLUSIONS

In summary, we successfully prepared the new $PbBiO_2Br$–SOF-$NbSe_2$ nanocomposite by a simple blending method (see Scheme 1 for image of the proposed mechanism). We found that the introduction of SOF-$NbSe_2$ could significantly enhance the higher photocatalytical activity of $PbBiO_2Br$ in the enantioselective α-alkylation of aldehyde, though overloading of the SOF-$NbSe_2$ would result in a decrease in its catalytic performance. We propose that the metallic SOF-$NbSe_2$ can be used as an efficient electron transfer support to suppress the recombination of photoinduced electron–hole pairs and contribute to the higher photocatalytic performance of the semiconductors in visible light photoredox catalysis.

Table 2. Enantioselective Alkylations Using Different Substrates

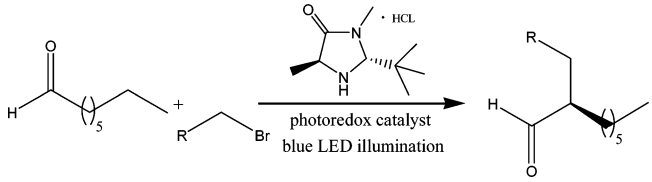

R	photoredox catalyst	yield [%]	ee [%]
−(C═O)Ph	$PbBiO_2Br$	53.5	96
−(C═O)Ph	$PbBiO_2Br$–0.5%SOF-$NbSe_2$	72.2	94
2,4-$(NO_2)_2$—C_6H_3	$PbBiO_2Br$	57.2	79
2,4-$(NO_2)_2$—C_6H_3	$PbBiO_2Br$–0.5%SOF-$NbSe_2$	81.5	81

ASSOCIATED CONTENT

Supporting Information

SEM images of SOF-$NbSe_2$ and $PbBiO_2Br$–SOF-$NbSe_2$ nanocomposite; TEM images of $PbBiO_2Br$–SOF-$NbSe_2$ composite and corresponding EDX element mappings of Se, Nb, Bi, Pb and Br; illustration for the proposed Se–Pb and Se–Bi bonds; TEM images of $PbBiO_2Br$–SOF-$NbSe_2$ with different mass ratios; band gap of $PbBiO_2Br$, and valence band of $NbSe_2$ according to the previous reports; diffuse reflectance UV–vis spectra of $PbBiO_2Br$, $PbBiO_2Br$–SOF-$NbSe_2$ and SOF-$NbSe_2$; TEM images of $PbBiO_2Br$–SOF-$NbSe_2$ and $PbBiO_2Br$-SOF-$NbSe_2$ reused; ^1H NMR of the product: diethyl 2-(1-oxohexan-2-yl)propanedioate; experimental data for the synthesis of (*R*)-2-(2-oxo-2-phenylethyl)hexanal and (*R*)-2-(2,4-dinitrobenzyl)octanal. This material is available free of charge via the Internet at http://pubs.acs.org.

AUTHOR INFORMATION

Corresponding Author

*Xiaobin Fan. Tel: (+86) 22-27890090. E-mail: xiaobinfan@tju.edu.cn.

Author Contributions

All authors have given approval to the final version of the paper.

Notes

The authors declare no competing financial interest.

ACKNOWLEDGMENTS

This study was supported by the National Natural Science Funds for Excellent Young Scholars (no. 21106099), Foundation for the Author of National Excellent Doctoral Dissertation of China (no. 201251), the Tianjin Natural Science Foundation (no. 11JCYBJC01700) and the Program of Introducing Talents of Discipline to Universities (no. B06006).

ABBREVIATIONS

2D = two-dimensional
EDX = energy dispersive X-ray spectroscopy
EIS = electrochemical impedance spectroscopy
HRTEM = high-resolution transmission electron microscopy
NMR = nuclear magnetic resonance
SEM = scanning electron microscopy
SOF = single- or few-layer
TEM = transmission electron microscopy
XRD = X-ray diffraction
UV–vis = UV–visible

DOI: 10.1021/acssuschemeng.5b00182
ACS Sustainable Chem. Eng. 2015, 3, 1017–1022

REFERENCES

(1) Prier, C. K.; Rankic, D. A.; MacMillan, D. W. C. Visible light photoredox catalysis with transition metal complexes: Applications in organic synthesis. *Chem. Rev.* **2013**, *113* (7), 5322−5363.

(2) Lin, W.-C.; Yang, D.-Y. Visible light photoredox catalysis: Synthesis of indazolo[2,3-a]quinolines from 2-(2-nitrophenyl)-1,2,3,4-tetrahydroquinolines. *Org. Lett.* **2013**, *15* (18), 4862−4865.

(3) Gao, X.-W.; Meng, Q.-Y.; Xiang, M.; Chen, B.; Feng, K.; Tung, C.-H.; Wu, L.-Z. Combining visible light catalysis and transition metal catalysis for the alkylation of secondary amines. *Adv. Synth. Catal.* **2013**, *355* (11−12), 2158−2164.

(4) Jiang, H.; Cheng, Y.; Wang, R.; Zhang, Y.; Yu, S. Synthesis of isoquinolines via visible light-promoted insertion of vinyl isocyanides with diaryliodonium salts. *Chem. Commun.* **2014**, *50* (46), 6164−6167.

(5) Feng, Z.-J.; Xuan, J.; Xia, X.-D.; Ding, W.; Guo, W.; Chen, J.-R.; Zou, Y.-Q.; Lu, L.-Q.; Xiao, W.-J. Direct sp^3 C-H acroleination of N-aryl-tetrahydroisoquinolines by merging photoredox catalysis with nucleophilic catalysis. *Org. Biomol. Chem.* **2014**, *12* (13), 2037−2040.

(6) Furst, L.; Narayanam, J. M. R.; Stephenson, C. R. J. Total synthesis of (+)-gliocladin C enabled by visible-light photoredox catalysis. *Angew. Chem., Int. Ed.* **2011**, *50* (41), 9655−9659.

(7) Xuan, J.; Xia, X.-D.; Zeng, T.-T.; Feng, Z.-J.; Chen, J.-R.; Lu, L.-Q.; Xiao, W.-J. Visible-light-induced formal [3+2] cycloaddition for pyrrole synthesis under metal-free conditions. *Angew. Chem.* **2014**, *126* (22), 5759−5762.

(8) Zhou, H.; Lu, P.; Gu, X.; Li, P. Visible-light-mediated nucleophilic addition of an α-aminoalkyl radical to isocyanate or isothiocyanate. *Org. Lett.* **2013**, *15* (22), 5646−5649.

(9) Zhu, Y.; Zhang, L.; Luo, S. Asymmetric α-photoalkylation of β-ketocarbonyls by primary amine catalysis: facile access to acyclic all-carbon quaternary stereocenters. *J. Am. Chem. Soc.* **2014**, *136* (42), 14642−14645.

(10) Wu, P.; He, C.; Wang, J.; Peng, X.; Li, X.; An, Y.; Duan, C. Photoactive chiral metal−organic frameworks for light-driven asymmetric α-alkylation of aldehydes. *J. Am. Chem. Soc.* **2012**, *134* (36), 14991−14999.

(11) Nicewicz, D. A.; MacMillan, D. W. C. Merging photoredox catalysis with organocatalysis: The direct asymmetric alkylation of aldehydes. *Science* **2008**, *322* (5898), 77−80.

(12) Lang, X.; Chen, X.; Zhao, J. Heterogeneous visible light photocatalysis for selective organic transformations. *Chem. Soc. Rev.* **2014**, *43* (1), 473−486.

(13) Melchiorre, P. Light in aminocatalysis: The asymmetric intermolecular α-alkylation of aldehydes. *Angew. Chem., Int. Ed.* **2009**, *48* (8), 1360−1363.

(14) Müller, C.; Bach, T. Chirality control in photochemical reactions: Enantioselective formation of complex photoproducts in solution. *Aust. J. Chem.* **2008**, *61* (8), 557−564.

(15) Nagib, D. A.; Scott, M. E.; MacMillan, D. W. C. Enantioselective α-trifluoromethylation of aldehydes via photoredox organocatalysis. *J. Am. Chem. Soc.* **2009**, *131* (31), 10875−10877.

(16) Shih, H.-W.; Vander Wal, M. N.; Grange, R. L.; MacMillan, D. W. C. Enantioselective α-benzylation of aldehydes via photoredox organocatalysis. *J. Am. Chem. Soc.* **2010**, *132* (39), 13600−13603.

(17) Nicewicz, D. A.; Nguyen, T. M. Recent applications of organic dyes as photoredox catalysts in organic synthesis. *ACS Catal.* **2013**, *4* (1), 355−360.

(18) Du, J.; Skubi, K. L.; Schultz, D. M.; Yoon, T. P. A dual-catalysis approach to enantioselective [2 + 2] photocycloadditions using visible light. *Science* **2014**, *344* (6182), 392−396.

(19) Noble, A.; MacMillan, D. W. C. Photoredox α-vinylation of α-amino acids and *N*-aryl amines. *J. Am. Chem. Soc.* **2014**, *136* (33), 11602−11605.

(20) Pan, Y.; Wang, S.; Kee, C. W.; Dubuisson, E.; Yang, Y.; Loh, K. P.; Tan, C.-H. Graphene oxide and rose bengal: Oxidative C-H functionalisation of tertiary amines using visible light. *Green Chem.* **2011**, *13* (12), 3341−3344.

(21) Maity, S.; Zhu, M.; Shinabery, R. S.; Zheng, N. Intermolecular [3+2] cycloaddition of cyclopropylamines with olefins by visible-light photocatalysis. *Angew. Chem., Int. Ed.* **2012**, *51* (1), 222−226.

(22) Griesbeck, A. G. Organic synthesis using photoredox catalysis. *Beilstein J. Org. Chem.* **2014**, *10*, 1097−1098.

(23) Wang, J.; Ma, J.; Li, X.; Li, Y.; Zhang, G.; Zhang, F.; Fan, X. Cu_2O mesoporous spheres with a high internal diffusion capacity and improved catalytic ability for the aza-Henry reaction driven by visible light. *Chem. Commun.* **2014**, *50* (91), 14237−14240.

(24) Cherevatskaya, M.; Neumann, M.; Füldner, S.; Harlander, C.; Kümmel, S.; Dankesreiter, S.; Pfitzner, A.; Zeitler, K.; König, B. Visible-light-promoted stereoselective alkylation by combining heterogeneous photocatalysis with organocatalysis. *Angew. Chem., Int. Ed.* **2012**, *51* (17), 4062−4066.

(25) Riente, P.; Matas Adams, A.; Albero, J.; Palomares, E.; Pericàs, M. A. Light-driven organocatalysis using inexpensive, nontoxic Bi_2O_3 as the photocatalyst. *Angew. Chem., Int. Ed.* **2014**, *53* (36), 9613−9616.

(26) Zhang, H.; Lv, X.; Li, Y.; Wang, Y.; Li, J. P25-graphene composite as a high performance photocatalyst. *ACS Nano* **2009**, *4* (1), 380−386.

(27) Woan, K.; Pyrgiotakis, G.; Sigmund, W. Photocatalytic carbon-nanotube−TiO_2 composites. *Adv. Mater.* **2009**, *21* (21), 2233−2239.

(28) Wang, C.-y.; Pagel, R.; Bahnemann, D. W.; Dohrmann, J. K. Quantum yield of formaldehyde formation in the presence of colloidal TiO_2-based photocatalysts: Effect of intermittent illumination, platinization, and deoxygenation. *J. Phys. Chem. B* **2004**, *108* (37), 14082−14092.

(29) Vinodgopal, K.; Hotchandani, S.; Kamat, P. V. Electrochemically assisted photocatalysis: Titania particulate film electrodes for photocatalytic degradation of 4-chlorophenol. *J. Phys. Chem.* **1993**, *97* (35), 9040−9044.

(30) Liang, Y.; Wang, H.; Sanchez Casalongue, H.; Chen, Z.; Dai, H. TiO_2 nanocrystals grown on graphene as advanced photocatalytic hybrid materials. *Nano Res.* **2010**, *3* (10), 701−705.

(31) Perera, S. D.; Mariano, R. G.; Vu, K.; Nour, N.; Seitz, O.; Chabal, Y.; Balkus, K. J. Hydrothermal synthesis of graphene-TiO_2 nanotube composites with enhanced photocatalytic activity. *ACS Catal.* **2012**, *2* (6), 949−956.

(32) Sun, Z.; Guo, J.; Zhu, S.; Mao, L.; Ma, J.; Zhang, D. A high-performance Bi_2WO_6-graphene photocatalyst for visible light-induced H_2 and O_2 generation. *Nanoscale* **2014**, *6* (4), 2186−2193.

(33) Kim, C. H.; Kim, B.-H.; Yang, K. S. TiO_2 nanoparticles loaded on graphene/carbon composite nanofibers by electrospinning for increased photocatalysis. *Carbon* **2012**, *50* (7), 2472−2481.

(34) Pan, X.; Zhao, Y.; Liu, S.; Korzeniewski, C. L.; Wang, S.; Fan, Z. Comparing graphene-TiO_2 nanowire and graphene-TiO_2 nanoparticle composite photocatalysts. *ACS Appl. Mater. Interfaces* **2012**, *4* (8), 3944−3950.

(35) Du, J.; Lai, X.; Yang, N.; Zhai, J.; Kisailus, D.; Su, F.; Wang, D.; Jiang, L. Hierarchically ordered macro−mesoporous TiO_2−graphene composite films: Improved mass transfer, reduced charge recombination, and their enhanced photocatalytic activities. *ACS Nano* **2010**, *5* (1), 590−596.

(36) Li, B.; Liu, T.; Wang, Y.; Wang, Z. ZnO/graphene-oxide nanocomposite with remarkably enhanced visible-light-driven photocatalytic performance. *J. Colloid Interface Sci.* **2012**, *377* (1), 114−121.

(37) Xiang, G.; Li, T.; Zhuang, J.; Wang, X. Large-scale synthesis of metastable TiO_2(B) nanosheets with atomic thickness and their photocatalytic properties. *Chem. Commun.* **2010**, *46* (36), 6801−6803.

(38) Xiang, G.; Wu, D.; He, J.; Wang, X. Acquired pH-responsive and reversible enrichment of organic dyes by peroxide modified ultrathin TiO_2 nanosheets. *Chem. Commun.* **2011**, *47* (41), 11456−11458.

(39) Coleman, J. N.; Lotya, M.; O'Neill, A.; Bergin, S. D.; King, P. J.; Khan, U.; Young, K.; Gaucher, A.; De, S.; Smith, R. J.; Shvets, I. V.; Arora, S. K.; Stanton, G.; Kim, H.-Y.; Lee, K.; Kim, G. T.; Duesberg, G. S.; Hallam, T.; Boland, J. J.; Wang, J. J.; Donegan, J. F.; Grunlan, J. C.; Moriarty, G.; Shmeliov, A.; Nicholls, R. J.; Perkins, J. M.; Grieveson, E. M.; Theuwissen, K.; McComb, D. W.; Nellist, P. D.; Nicolosi, V. Two-

DOI: 10.1021/acssuschemeng.5b00182
ACS Sustainable Chem. Eng. 2015, 3, 1017−1022

dimensional nanosheets produced by liquid exfoliation of layered materials. *Science* **2011**, *331* (6017), 568−571.
(40) Zeng, Z.; Sun, T.; Zhu, J.; Huang, X.; Yin, Z.; Lu, G.; Fan, Z.; Yan, Q.; Hng, H. H.; Zhang, H. An effective method for the fabrication of few-layer-thick inorganic nanosheets. *Angew. Chem., Int. Ed.* **2012**, *51* (36), 9052−9056.
(41) Smith, R. J.; King, P. J.; Lotya, M.; Wirtz, C.; Khan, U.; De, S.; O'Neill, A.; Duesberg, G. S.; Grunlan, J. C.; Moriarty, G.; Chen, J.; Wang, J.; Minett, A. I.; Nicolosi, V.; Coleman, J. N. Large-scale exfoliation of inorganic layered compounds in aqueous surfactant solutions. *Adv. Mater.* **2011**, *23* (34), 3944−3948.
(42) Li, J.-M. Mass production of graphene-like single-crystalline $NbSe_2$ (004) nanosheets via intercalant-assisted thermal cleavage. *Appl. Phys. A: Mater. Sci. Process.* **2010**, *99* (1), 229−235.
(43) Zeng, Z.; Yin, Z.; Huang, X.; Li, H.; He, Q.; Lu, G.; Boey, F.; Zhang, H. Single-layer semiconducting nanosheets: High-yield preparation and device fabrication. *Angew. Chem., Int. Ed.* **2011**, *50* (47), 11093−11097.
(44) Graham, T. H.; Horning, B. D.; MacMillan, D. W. C. The preparation of (2*R*,5*S*)-2-*t*-butyl-3,5-dimethylimidazolidin-4-one. *Org. Synth.* **2003**, 42−53.
(45) Zhang, H.; Wang, G.; Chen, D.; Lv, X.; Li, J. Tuning photoelectrochemical performances of Ag−TiO_2 nanocomposites via reduction/oxidation of Ag. *Chem. Mater.* **2008**, *20* (20), 6543−6549.
(46) Fan, W.; Lai, Q.; Zhang, Q.; Wang, Y. Nanocomposites of TiO_2 and reduced graphene oxide as efficient photocatalysts for hydrogen evolution. *J. Phys. Chem. C* **2011**, *115* (21), 10694−10701.
(47) He, B.-L.; Dong, B.; Li, H.-L. Preparation and electrochemical properties of Ag-modified TiO_2 nanotube anode material for lithium−ion battery. *Electrochem. Commun.* **2007**, *9* (3), 425−430.
(48) Zhang, Z. C.; Xu, B.; Wang, X. Engineering nanointerfaces for nanocatalysis. *Chem. Soc. Rev.* **2014**, *43* (22), 7870−86.
(49) Chen, G. X.; Yang, H. Y.; Wu, B. H.; Zheng, Y. P.; Zheng, N. F. Supported monodisperse Pt nanoparticles from $[Pt_3(CO)_3(\mu_2\text{-}CO)_3]_5^{2-}$ clusters for investigating support-Pt interface effect in catalysis. *Dalton Trans.* **2013**, *42* (35), 12699−12705.

DOI: 10.1021/acssuschemeng.5b00182
ACS Sustainable Chem. Eng. 2015, 3, 1017−1022